

Accounts

Synthesis and Properties of Liquid-Crystalline-Conjugated Polymers

Kazuo Akagi

Department of Polymer Chemistry, Graduate School of Engineering, Kyoto University, Katsura, Nishikyo-ku, Kyoto 615-8510

Received March 7, 2006; E-mail: akagi@star.polym.kyoto-u.ac.jp

We have synthesized novel liquid-crystalline (LC)-conducting polymers by introducing LC groups into acetylene monomers and polymerizing them with Ziegler–Natta, metathesis, and rhodium-based catalysts. All polymers prepared were soluble in organic solvents and had a thermotropic liquid crystallinity characterized with fan-shaped texture in polarizing optical microscopy. Phase transitions and the corresponding enthalpy changes were also evaluated by means of differential scanning calorimeter (DSC). High-order structures of the polymers were investigated by means of X-ray diffraction (XRD) analyses. XRD measurements showed that the polymers had layered structures in the LC state to give smectic A phases, which is in agreement with the results from the polarizing optical microscope. We found that the LC side chains alternate on both sides of the polyene chain, giving rise to a stereoregular sequence, such as head–head–tail–tail linkage. Macroscopic alignments of the polymers were performed in the liquid-crystalline phase by shear stress or a magnetic force field of 0.7–1.0 Tesla, which resulted in an enhancement by two orders of magnitude in the electrical conductivity of iodine-doped cast films. Orientation behaviors of the polymers as well as the monomers were investigated using fused-state ^{13}C NMR measurements with proton dipolar decoupling. Analysis of chemical shift tensors was also carried out to evaluate the order parameter and shielding anisotropy in the LC phase. As a result, we demonstrated that LC-conjugated polymers uniaxially aligned due to the magnetically forced alignment of the LC side-chain, giving rise to a monodomain structure.

1. Introduction

Among a variety of electrically conducting polymers reported so far, polyacetylene is the most typical conjugated polymer that has been studied,¹ and it has the highest electrical conductivity in the order of 10^4 – 10^5 S cm^{-1} upon an iodine doping.² However, it is insoluble and infusible, which makes it difficult to determine its molecular weight and chemical structure and to process the polymer in solution, such as casting. Introduction of alkyl or aromatic substituents onto the polyacetylene chain makes the polymer soluble in organic solvents, when the alkyl chain length is sufficiently long, i.e., hexyl, pentyl, and octyl groups.³ Electrical conductivity of substituted polyacetylene, however, is significantly lower than that of non-substituted polyacetylene. This is due to less coplanarity of the main chain arising from steric repulsions between substituents as well as a higher ionization potential and a lower electron affinity. In addition, even in the substituted polyacetylene, the main chain is still randomly oriented, which suppressed the observed electrical conductivity of the polymer.

If the substituent is a liquid-crystalline (LC) group, the polymer is not only soluble in organic solvents, but also easily aligned by spontaneous orientation of the LC group. Besides, it could be macroscopically aligned by an external perturbation, such as shear stress, electric or magnetic force field. This

situation means that a monodomain structure of the LC phase can be constructed on a macroscopic level. Thus, the polymer should have a higher electrical conductivity, compared with the case of random orientation. At the same time, one can control the molecular orientation, and hence the electrical conductivity of the polymers with an external force. Figure 1 shows schematically both spontaneous orientation and externally forced macroscopic alignment of side chain type LC-conjugated polymers, where the former and the latter generate multi and mono domains of LC phases, respectively. Currently, a series of LC polyacetylene derivatives have been synthesized and characterized from aspects of thermal and electrical properties.⁴ For these novel LC-conducting polymers, the macroscopic alignment has been first achieved under magnetic force field.^{4c} Since it is possible to prepare a variety of LC-conducting polymers, it is straightforward to study other kinds of conjugated polymers. In fact, following LC polyacetylene derivatives, which are to be reviewed in more details, various types of LC polymers have been synthesized over the last few decades. Scheme 1 shows representative LC-conducting polymers, e.g., LC polyene derivatives with a six-membered cyclic backbone structures, such as poly(1,6-heptadiyne) and poly(dipropargylamine),⁵ polythiophene derivatives with mesogenic groups at 3-position of thiophene rings,⁶ LC polypyrrole derivatives with mesogenic groups at 3-position or *N*-position of

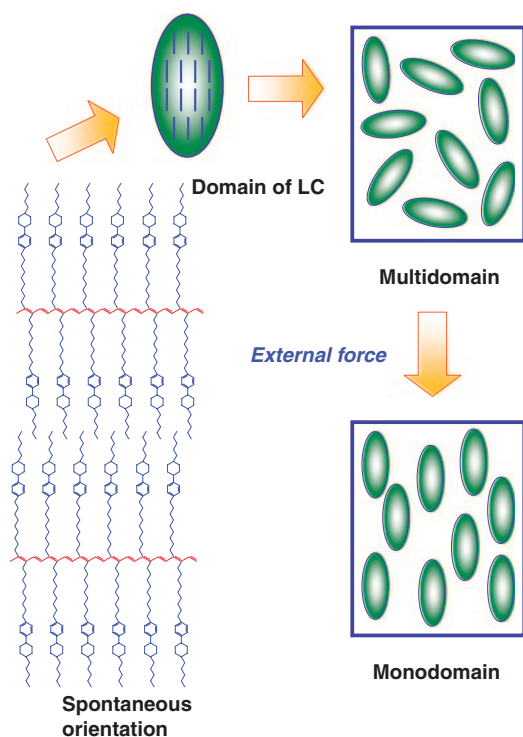


Fig. 1. Schematic representation of spontaneous and magnetically forced orientations of side chain LC-conjugated polymer.

pyrrole rings,⁷ LC poly(*para*-phenylene) derivatives,⁸ LC poly(*para*-phenylenevinylene) derivatives,⁸ LC polythienylenevinylene derivatives with mesogenic groups at phenylene or thiophene rings,⁹ LC polyaniline derivatives with mesogenic groups at ortho-position of aniline ring.¹⁰ In addition, small-band gap LC-conjugated polymers¹¹ based on benzenoid and quinoid resonance structures were synthesized. Subsequently, ferroelectric LC (FLC)-conjugated polymers¹² consisting of acetylene, thiophene, phenylene, or phenylenevinylene unit cell were synthesized in order to achieve highly quick response to an electric force field during macroscopic alignment. FLC-conjugated polymers are reviewed elsewhere.

1.1 LC Polyacetylene Derivatives.^{4,13–18} The LC substituent on the monomer was composed of a phenylcyclohexyl (PCH) moiety as a mesogenic core, methylene chain linked with an ether-type oxygen atom, $-(\text{CH}_2)_3\text{O}$, as a spacer, and an alkyl chain $(-\text{C}_n\text{H}_{2n+1})$, $n = 2, 3,$ and $5-8$ as a terminal group, and the monomer is abbreviated as PCH n 03A, where A stands for acetylene segment. Another LC substituent consists of a biphenyl (BP) mesogenic core, a methylene chain linked with oxygen as a spacer, and an n -pentyl group as a terminal moiety. In this case, the monomer is abbreviated as BP n 03A ($n = 5$). The monomers were polymerized with Ziegler–Natta, metathesis, and rhodium-based catalysts. The corresponding polymers are abbreviated as PPCH n 03A and PBP n 03A, as shown in Scheme 2.

The present monomers and polymers were characterized by means of infrared (IR), UV–vis, ¹H and ¹³C nuclear magnetic resonance (NMR) spectroscopies, elemental analyses, DSC, and polarizing optical microscopy. Molecular weights of the polymers were evaluated by means of gel-permeation chroma-

tography (GPC) using polystyrene standards, and electrical conductivities upon iodine doping of cast films of the polymers were measured by using a four-probe method. Morphologies were examined through measurements of scanning electron microscopy (SEM).

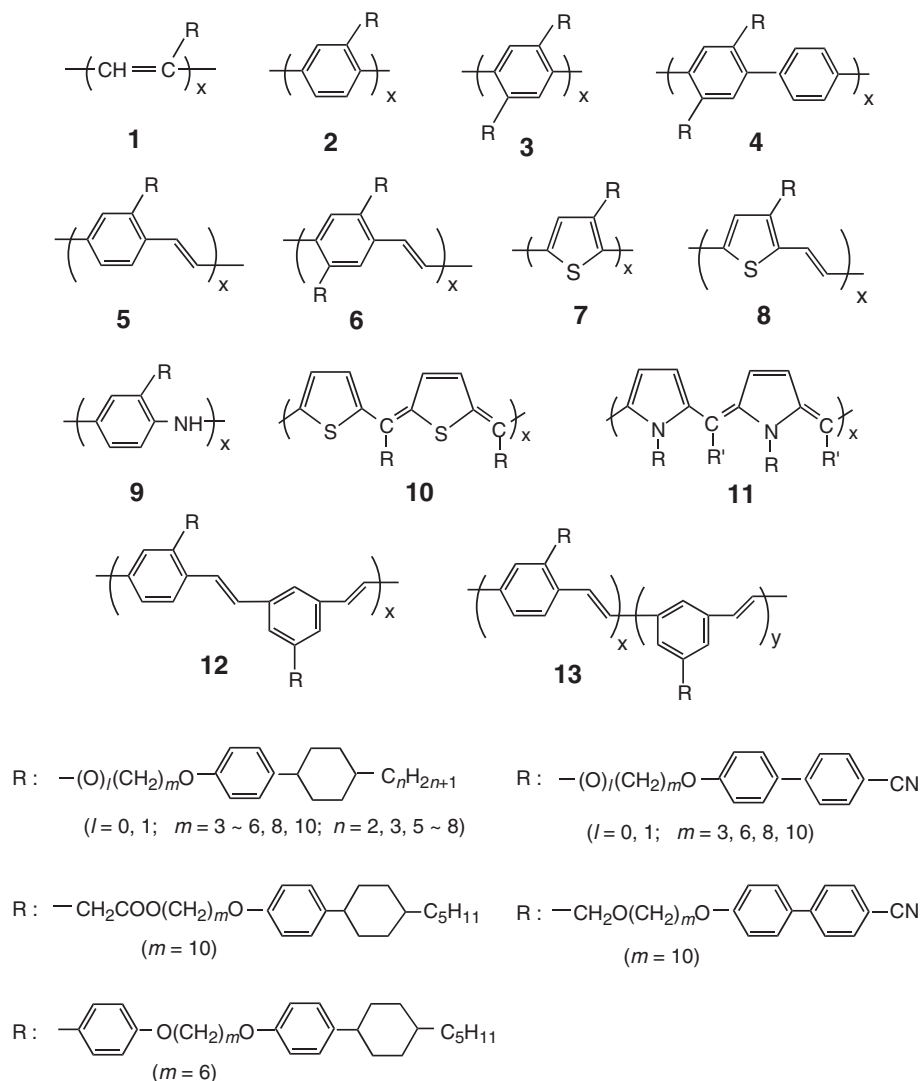
2. Preparation

2.1 Syntheses of Monomers. (i) The PCH n 03A was synthesized by reacting *para*-(*trans*-4-alkylcyclohexyl)phenol and 5-chloro-1-pentyne in sodium ethoxide by using potassium iodide as a catalyst (Scheme 3). (ii) Four steps to synthesize BP503A were necessary. First, 4-methoxy-4'-pentanoylbiphenyl (**1**) was synthesized through a Friedel–Crafts reaction between 4-methoxybiphenyl and pentanoyl chloride in nitrobenzene using aluminium chloride as a catalyst. The carbonyl moiety of **1** was reduced to a methylene group by hydrazine and potassium hydroxide in diethylene glycol to yield 4-methoxy-4'-pentylbiphenyl (**2**). The methoxy group of **2** was changed into a hydroxy group using hydrogen bromide in acetic acid and tetra-*n*-butylammonium bromide (TBAB). Etherification of the product 4'-pentyl-4-biphenylol (**3**) was carried out by coupling it with 5-chloro-1-pentyne in sodium ethoxide using potassium iodide as a catalyst, yielding BP503A (Scheme 3).

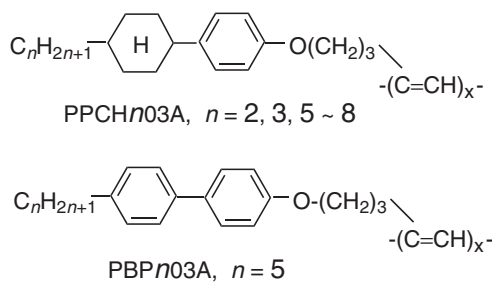
2.2 Polymerizations of Monomers. Polymerizations of PCH n 03A and BP503A were carried out by using a Ziegler–Natta catalyst,¹⁹ Fe(acac)₃–AlEt₃, and a metathesis catalyst,²⁰ MoCl₅–Ph₄Sn, in toluene for 21 h at room temperature. For some of the monomers, a chlorine-bridged rhodium complex,²¹ [Rh(NBD)Cl]₂, was used with NEt₃ as a co-catalyst, and the polymerization time was within 6 min at room temperature.^{4f–g} The polymerizations were terminated by pouring the reaction mixture into a large amount of methanol. The polymers were filtered off, washed with methanol and then dried under vacuum. The yields and molecular weights evaluated from GPC are summarized in Table 1. The MoCl₅–Ph₄Sn catalyst gave higher yields of the polymers than the Fe(acac)₃–AlEt₃ catalyst. The number-average molecular weight ($M_n = 10^5$) was higher for Fe-based PPCH803A. Although Fe-based PBP503A was insoluble in tetrahydrofuran (THF) and benzene in the range of room temperature to 90 °C, it was soluble in cumene upon heating up at 120 °C for 30 min. The dissolved polymer had a low viscosity and relatively small molecular weight ($3000 < M_n < 4000$). This may be due to decomposition during the heating process.

3. Properties

3.1 LC Phases of Monomers. Liquid crystallinity of PCH n 03A was determined with a miscibility test. Figure 2 shows a phase diagram of a mixture of PCH803A and 1-hexyloxy-4-(*trans*-4-propylcyclohexyl)benzene, PCH306. The latter is known to have a nematic LC phase and, therefore, is used as a reference. In the miscibility phase diagram, the mixture is homogeneous irrespective of the mole ratio between the two compounds. This indicates that the LC phase of PCH803A is nematic. The result is supported by the experimental facts that PCH803A had a mesophase in DSC and it had a Schlieren texture characteristic of a nematic phase under a polarizing optical microscope. Similarly, PCH n 03A with $n = 5-7$ were also



Scheme 1.



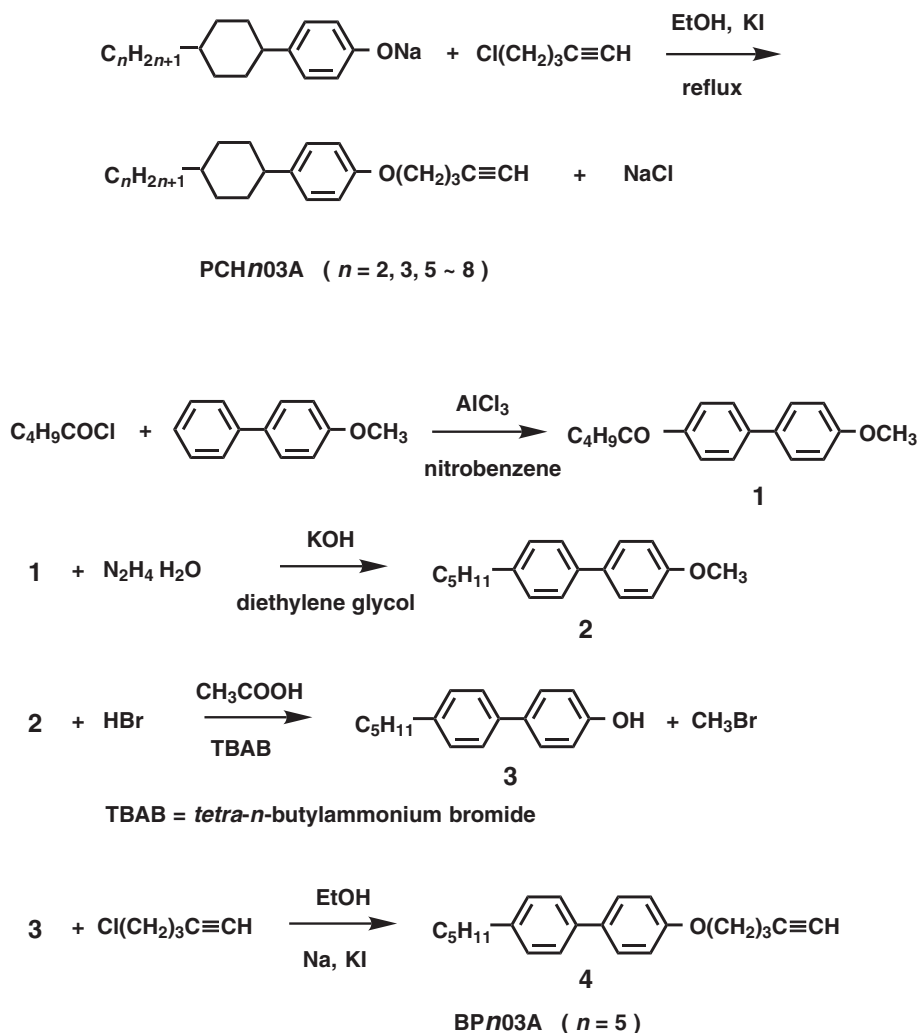
Scheme 2.

confirmed to have nematic LC phases. It should be noted that the above-mentioned mesophases of the monomers were observed only during the cooling process, indicating that the monomers are monotropic liquid crystals.

3.2 Liquid-Crystalline Phases of Polymers. All PCH and BP polymers with LC groups in the side chain had fan-shaped textures and uniaxial conoscopic patterns under a polarizing optical microscope that are characteristic of a smectic A phase. Typical fan-shaped textures of the polymers prepared with Fe-based and Mo-based catalysts are shown in Fig. 3. It was

found that the domain size of the LC phase increased with an increase in terminal alkyl chain length of the side-chain of the PCH polymer. In addition, the domain size of the Mo-based PBP503A polymer was larger than that of the Fe-based polymer. This is consistent with the experimental fact that the latter is thermally more stable than the former.

DSC measurements of the polymers were carried out, as shown in Fig. 4. It has been recently reported that the PCH and BP polymers prepared with a Ziegler–Natta catalyst, such as $\text{Fe}(\text{acac})_3\text{-AlEt}_3$, assume a cis form, while those obtained with a metathesis catalyst, such as $\text{MoCl}_5\text{-Ph}_4\text{Sn}$, exhibit a trans form.¹³ Fe-based PPCH803A exhibited a large exothermic peak due to a cis–trans isomerization between 150 and 190 °C in the first heating process. An endothermic peak around 170 °C was hidden by the isomerization peak. During the first cooling period, a peak corresponding to an isotropic to liquid crystal phase transition was observed at 146 °C, and that corresponding to liquid crystal to solid phase transition at 98 °C. During the second heating period, the liquid-crystal phase was observed in the temperature range of 100–128 °C. Phase-transition temperatures and enthalpy changes of some



Scheme 3.

Table 1. Polymerization Yields and Molecular Weights of PPCH n 03A and PBP503A Prepared with Fe(acac)₃-AlEt₃ and MoCl₅-Ph₄Sn Catalysts (acac = acetylacetonate)

Polymer ^{a)}	Fe(acac) ₃ -AlEt ₃ ^{b)}				MoCl ₅ -Ph ₄ Sn ^{c)}			
	Yield /%	M_n	M_w	M_w/M_n	Yield /%	M_n	M_w	M_w/M_n
PPCH303A	71	5.5×10^5	2.6×10^6	4.7	61	1.5×10^4	3.4×10^4	2.3
PPCH503A	70	4.5×10^5	1.8×10^6	4.0	67	1.4×10^4	3.3×10^4	2.4
PPCH803A	67	5.2×10^5	2.6×10^6	5.0	73	1.2×10^4	2.7×10^4	2.3
PBP503A	65	3.5×10^3	1.0×10^4	2.9	85	7.5×10^3	6.8×10^4	9.1

a) Polymerized in toluene for 21 h at room temperature. [Monomer] = 3 mmol, [Fe(acac)₃] = 0.01 mol L⁻¹, [AlEt₃]/[Fe(acac)₃] = 6, [MoCl₅] = 0.01 mol L⁻¹, [Ph₅Sn]/[MoCl₅] = 0.5. b) Polymers are soluble in organic solvents such as CHCl₃, THF, and benzene at 50–60 °C. For the measurements of GPC spectra, the polymers were first dissolved in THF with heating and then allowed to cool to room temperature. c) Polymers are soluble in the same solvents as mentioned above at room temperature.

representative polymers are listed in Table 2. In the PCH polymer, the enthalpy change due to the smectic to isotropic phase transition increased with an increase in the terminal alkyl chain length. This means that the liquid-crystal state is more stabilized with longer the alkyl chains as the terminal moiety of the LC group. However, the stabilization of the liquid-crystal state of the BP polymer was relatively small compared with

the PCH polymer. Mesophases of the PPCH n 03A and PBP503A were observed in both heating and cooling processes. This indicates that the polymers, irrespective of the catalyst used in the polymerization, are enantiotropic liquid crystals. Here, it should be emphasized that PCH n 03A monomers ($n = 5\text{--}8$) had nematic phases, while all of the polymers had smectic phases of which the ordering was higher than that in

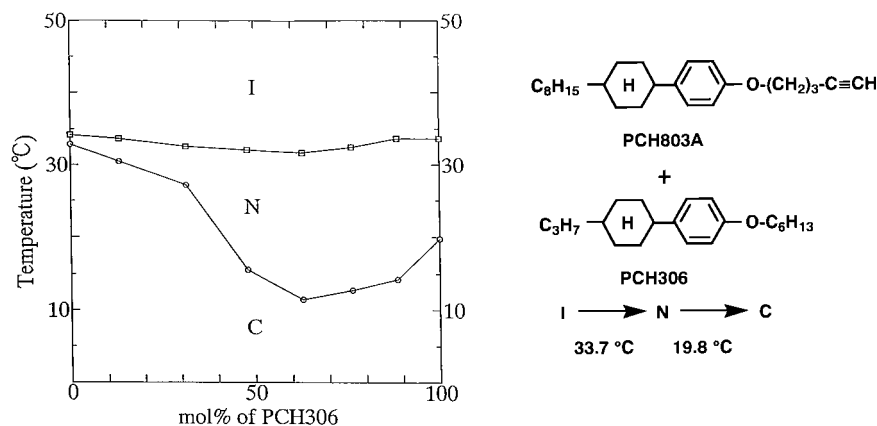


Fig. 2. Phase diagram of mixture of PCH803A and PCH306 (I = isotropic; N = nematic; C = crystalline).

the nematic phase. This can be rationalized by involving the so-called polymerization effect, i.e., higher ordering in molecular arrangement occurs due to the polymerization of the LC monomer.¹⁶

3.3 Higher Order Structure and Stereospecific Configuration. Figure 5 shows an XRD pattern of Fe-based PPCH503A. Two diffraction peaks, sharp and broad ones, were observed in small- and wide-angle regions, respectively. Such a XRD profile is usually observed for a smectic LC phase. Similar XRD patterns were also observed for the other LC polyacetylene derivatives studied here. The results of XRD analyses are summarized in Table 3. Diffractions of sharp and broad peaks were observed at 2.35 and 18.6° in 2 θ , respectively. These diffraction angles correspond to periodic distances of 37.5 and 4.76 Å, respectively. Namely, the former and the latter correspond to an inter-layer distance in the smectic state and the separation between side chains, respectively, as shown in Fig. 6a. These assignments were supported by molecular mechanics calculations based on finite systems of LC polyacetylene derivatives; the inter-layer distance and the side-chain separation were calculated to be 41 and 5 Å, respectively. The present analyses enabled us to draw a polymer structure of Fe-based PPCH503A where the LC side chains are alternatively located at both sides of polyene chain to form a stereoregular configuration of head-head-tail-tail linkage, as shown in Fig. 6b. At the same time, the polymer structure implied that the LC side chains are not tilted with respect to the main chain, leading to a typical picture of smectic A phase. It should be emphasized that the fully extended side chains are arrayed perpendicular to the linear backbone, alternatingly on both sides along it, and the alternating comb-like polymers are stacked into a layer structure. The terminal alkyl group of the side chain has a trans conformation. The cyclohexyl group is in a stable chair conformation. As found in the center and right sites of Fig. 6b, the chain conformation from C₃ through O to C₆ atom is gauche, and as a whole, the side chain is extended in an almost straight fashion. The side chain is twisted about the C₂-C₃ bond, so that the hydrogen atoms attached to the C₃ atom are directed upward from the figure plane (the plane containing the backbone), so as to release repulsions with the neighboring hydrogens of the backbone. About the C₂'-C₃' bond, the side chain is twisted in the opposite direction, so that the two mesogens are in the antipode arrangement

with respect to the intervening double bond.¹⁷ As shown in Table 3, all of the polymers have the side-chain separations of 4.6–4.8 Å. This implies that the side-chain separations are irrespective of differences in the LC substituents. Meanwhile, the inter-layer distance increased as the terminal alkyl chain or the methylene chain became longer; it increased by 6.4 Å from Mo-based PPCH503A to PPCH803A, or by 5.6 Å from Rh-based PPCH503A to PPCH506A. This also supports the present assignment that the sharp peak in the small angle region is due to diffraction between the inter-layers of smectic A form. As a typical example, a comparison of the inter-layer distances between Mo-based PPCH503A and PPCH803A is shown in Fig. 6c. It is clear that the increase in the inter-layer distance by 6.4 Å, which is twice the value of 3.2 Å, is due to the difference in length between the terminal pentyl and octyl groups of the side chains in the bi-layer type smectic A (S_{A2}) phase.

Here, it is worthwhile to determine how the above-mentioned stereoregular configuration is formed. Previous studies using ¹H NMR, DSC, and ESR^{13b} have confirmed that as-prepared LC polyacetylene derivatives with Fe- or Rh-based catalyst and Mo-based catalyst have cis and trans forms, respectively. The cis form is thermally unstable and is easily isomerized into the trans form during the first heating process in the DSC or polarizing optical microscope measurements. Taking this into account, we propose a possible polymerization and cis-trans isomerization mechanism in Fig. 7. The LC-substituted acetylene monomers approaching to a catalytically active site are polymerized with a sequence of head-head and tail-tail linkages, yielding a stereoregular cis form. In cases of Fe- or Rh-based catalysts, the cis form is a kinetic product, and hence it is converted into the trans form that is a thermodynamic product. In case of Mo-based catalyst, the cis to trans isomerization should occur simultaneously during the polymerization.

3.4 Absorption Spectra and Chemical Doping. Next, UV-vis absorption spectra of PCH503A and PPCH503A prepared with Fe-based catalyst were acquired. An absorption band between 270 and 280 nm for the monomer and the polymer was assigned to the $\pi \rightarrow \pi^*$ transition of the benzene moiety of the LC group. The absorption band between 320 and 330 nm in the polymer was assigned to the $\pi \rightarrow \pi^*$ transition in the conjugated polyene chain. Broadening of the band implies that the polymer is composed of finite polyenes with

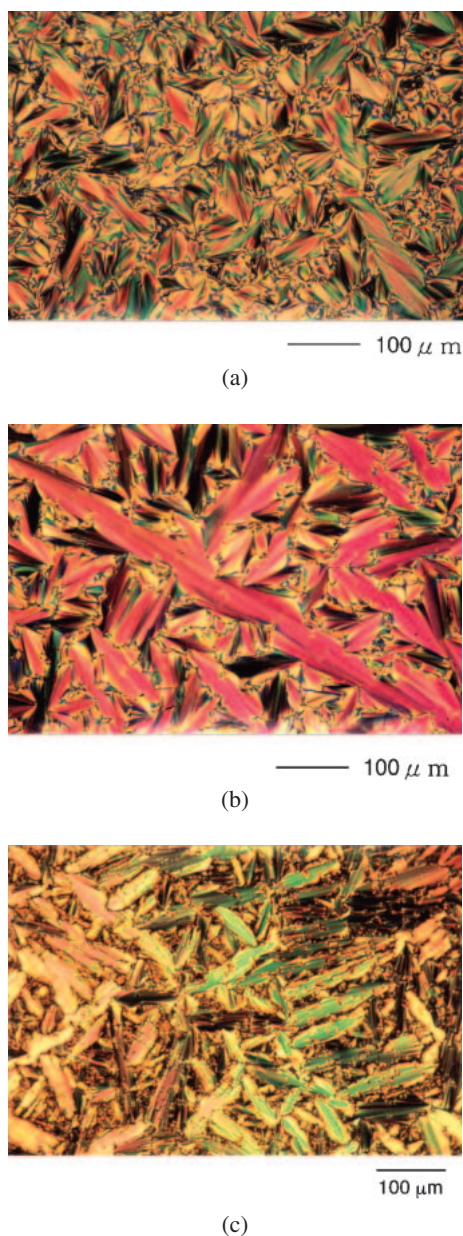


Fig. 3. Polarizing micrographs of PCH and BP polymers showing fan-shaped textures. (a) Fe-based PPCH803A at 132 °C; (b) Mo-based PPCH803A at 130 °C; (c) Mo-based PBP503A at 120 °C.

various conjugation lengths. The results from the absorption spectra for the representative polymers are summarized in Table 4. The Mo-based polymer had an absorption band located at shorter wavelength (around 300 nm) than the Fe-based polymer, indicating that the former has a shorter conjugation length in the polyene chain than the latter. It should be noted that the microscopic UV-vis measurement of the inside of the LC domain in Fe-based PPCH803A gave an absorption band at 403 nm, which is shifted by 70 nm towards a longer wavelength compared to the band observed in solution of the polymer.¹⁴ The result demonstrates that the polyene chains are aligned owing to the spontaneous orientation of the LC side chains and that the effective conjugation lengths of polyene chains inside of each domain are longer than those in a ran-

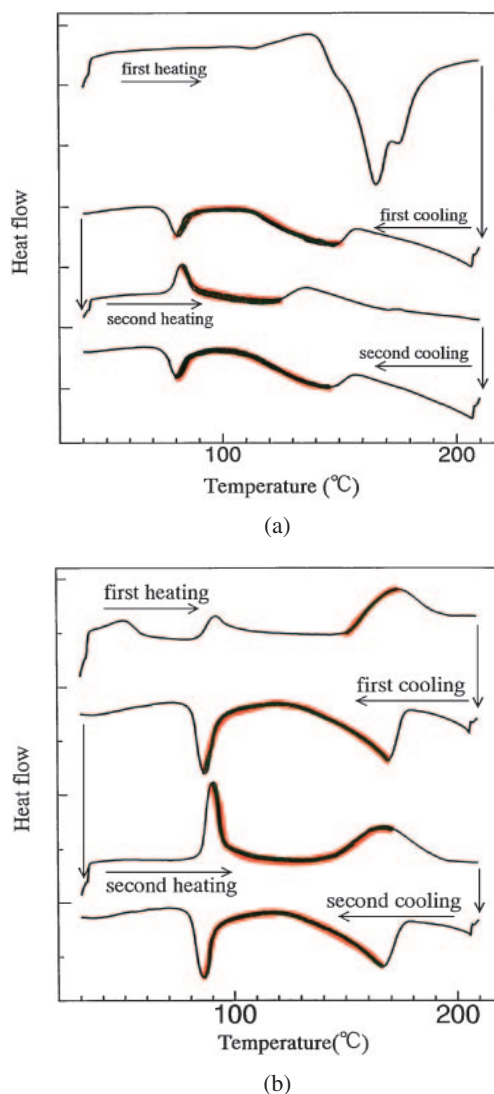


Fig. 4. DSC curves of PPCH803A polymers prepared with (a) $\text{Fe}(\text{acac})_3\text{-AlEt}_3$ and (b) $\text{MoCl}_5\text{-Ph}_4\text{Sn}$ catalysts. The rate of temperature change in the heating or cooling process was 5°C min^{-1} .

domly oriented case, such as in solution, probably due to an increase of co-planarity of the polyene chains. Therefore, from a view point of enhancement of electrical conductivity, a macroscopic alignment of the polymer that is a so-called mono domain structure of the LC state must occur via an external perturbation, as mentioned in the next section (see also Fig. 1).

Absorption spectra of Fe-based PPCH803A, which had been cast onto an inner wall of a quartz cell, were measured in situ after iodine doping. The results are shown in Fig. 8. Since the ionization potential of substituted polyacetylene is generally larger than that of non-substituted polyacetylene, it might take more time to complete the iodine doping of the polymers. Actually, there was no notable change in the absorption spectrum even after 3 h of exposure to iodine. After 5 h, the absorption band from 320 to 330 nm, assigned to a $\pi \rightarrow \pi^*$ transition in conjugated polyene, slightly decreased in intensity. At the same time, new bands appeared at 420 and 700 nm. Interestingly, these bands were also observed in gas-phase doping

with sulfuric acid. Therefore, the two bands originate from a chemically doped conjugated polyene chain and can be assigned to two kinds of electronically allowed transitions in positively charged polyene segments. Thus, it is possible to chemically dope the present polymers.

3.5 Molecular Orientation and Electrical Conductivity.

3.5.1 Orientation by Shear Stress: Figure 9 shows SEM photographs of Fe-based PPCH503A. Figure 9a shows randomly oriented fibrils. Figures 9b–9d show aligned fibrils that are generated by a shear stress along the horizontal direction of the paper in the LC state of the polymer. Figure 10a shows polarizing micrographs of Mo-based PPCH503A. It is evident that a batonet optical texture, characteristic of a smectic liquid crystal, is oriented along the direction of the shear stress. From these results, we confirmed that the side chain LC-conjugated polymers are macroscopically aligned by the shear stress as an external force.

3.5.2 Orientation by Magnetic Field: Electrical conductivity of the polymers was measured by using the four-probe method. The polymer was first melted onto a hot substrate on which gold had been vaporized in the form of four leads, and it was gradually cooled down to the LC temperature by applying an external magnetic field of 0.7–1.0 Tesla. After alignment of the polymer was completed in the LC state, the polymer was further cooled down to room temperature to give a

solid sample available for conductivity measurements. Schematic representation of the magnetically forced alignment of the polymer and current direction in the four-probe measurement are shown in Fig. 11, where σ_{\parallel} and σ_{\perp} stand for the conductivities parallel and perpendicular to the direction of the polymer main chain. The results are summarized in Table 5. Conductivities of undoped and iodine-doped samples were 10^{-11} – 10^{-9} and 10^{-8} – 10^{-7} S cm $^{-1}$, respectively. Through the magnetically forced alignment, the conductivity of the doped sample was further enhanced by 1–2 orders of magnitude to give 10^{-6} S cm $^{-1}$. Especially, the conductivity of the aligned sample of Fe-based PPCH503A increased 10^2 times in σ_{\parallel} , i.e., from 10^{-8} to 10^{-6} S cm $^{-1}$. As for PBP503A, the increase due to the alignment was only about 2 times.

Meanwhile, the σ_{\perp} of Mo-based PPCH503A and PBP503A decreased by 10^2 – 10^4 , as expected. However, those of Fe-based PPCH503A increased by 70 times. The difference in conductivity resulted in a wide range of electrical anisotropy ($\sigma_{\parallel}/\sigma_{\perp}$) (2 – 10^5).

The increase in σ_{\perp} after macroscopic alignment, as mentioned in the case of Fe-based PPCH503A may, in part, be due to an increase in the coplanarity of the conjugated polyene chain upon alignment. This suggests that in analyzing the change in conductivity upon the molecular orientation, an in-plane alignment of the polyene chain must be considered at the same time, as well as a so-called parallel alignment of the polyene chain.¹⁵

Figure 10a shows polarizing optical micrographs of Fe-based PPCH803A after magnetically forced alignment. The

Table 2. Phase-Transition Temperature (°C) and Enthalpy Changes (J g $^{-1}$) for PPCH*n*03A and PBP503A

Cat. ^{b)}	Polymer	First cooling ^{a)}		Second heating ^{a)}	
		k → S _A → i		k → S _A → i	
Fe	PPCH303A	60 (0.7)	107 (4.5)	70 (0.7)	102 (3.3)
	PPCH503A	98 (1.1)	146 (6.3)	100 (1.3)	128 (6.2)
	PPCH803A	81 (3.2)	151 (8.2)	83 (3.3)	142 (5.8)
	PBP503A	126 (3.2)	180 (3.1)	129 (4.9)	171 (1.0)
Mo	PPCH303A ^{c)}		133 (4.2)		134 (3.7)
	PPCH503A ^{c)}		160 (6.2)		160 (4.5)
	PPCH803A	86 (3.4)	171 (6.7)	91 (3.7)	166 (6.4)
	PBP503A	132 (4.4)	189 (4.5)	135 (6.7)	180 (—)

a) k = crystalline, S_A = smectic A, i = isotropic. b) Fe and Mo denote catalysts of Fe(acac)₃–AlEt₃ and MoCl₅–Ph₄Sn, respectively. c) No distinct DSC peak corresponding to the phase transition between crystalline and smectic A phases was observed.

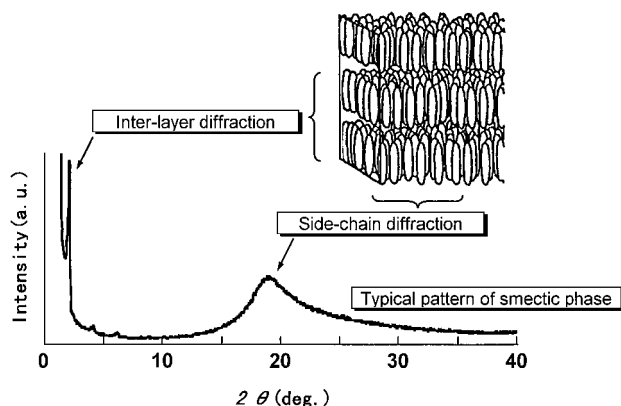


Fig. 5. X-ray diffraction pattern of Fe-based PPCH503A.

Table 3. XRD Results for LC Polyacetylene Derivatives

Polymer	Tail ^{a)}	Spacer ^{a)}	Catalyst ^{b)}	Isomerization ^{c)}	LC phase	Inter-layer distance/Å	Side-chain separation/Å
PPCH503A	5	3	Fe	cis → trans	S _A	37.5	4.76
			Rh	cis → trans	S _A	38.0	4.73
			Mo	trans	S _A	40.2	4.55
			(cal.) ^{d)}	—	—	(≈41) ^{d)}	(5.0) ^{d)}
PPCH506A	5	6	Rh	cis → trans	S _A	43.6	4.71
PPCH803A	8	3	Mo	trans	S _A	46.6	4.75

a) Number of the carbon atoms in the terminal alkyl moiety or methylene spacer moiety of LC side chain. b) Fe, Mo, and Rh denote catalysts of Fe(acac)₃–AlEt₃, MoCl₅–Ph₄Sn, and [Rh(NBD)Cl]₂–NEt₃, respectively. c) Fe- and Rh-based catalysts and Mo-based one give cis-rich and trans-rich polyacetylene derivatives, respectively. d) Values in the parenthesis are based on molecular mechanics calculations for finite systems.

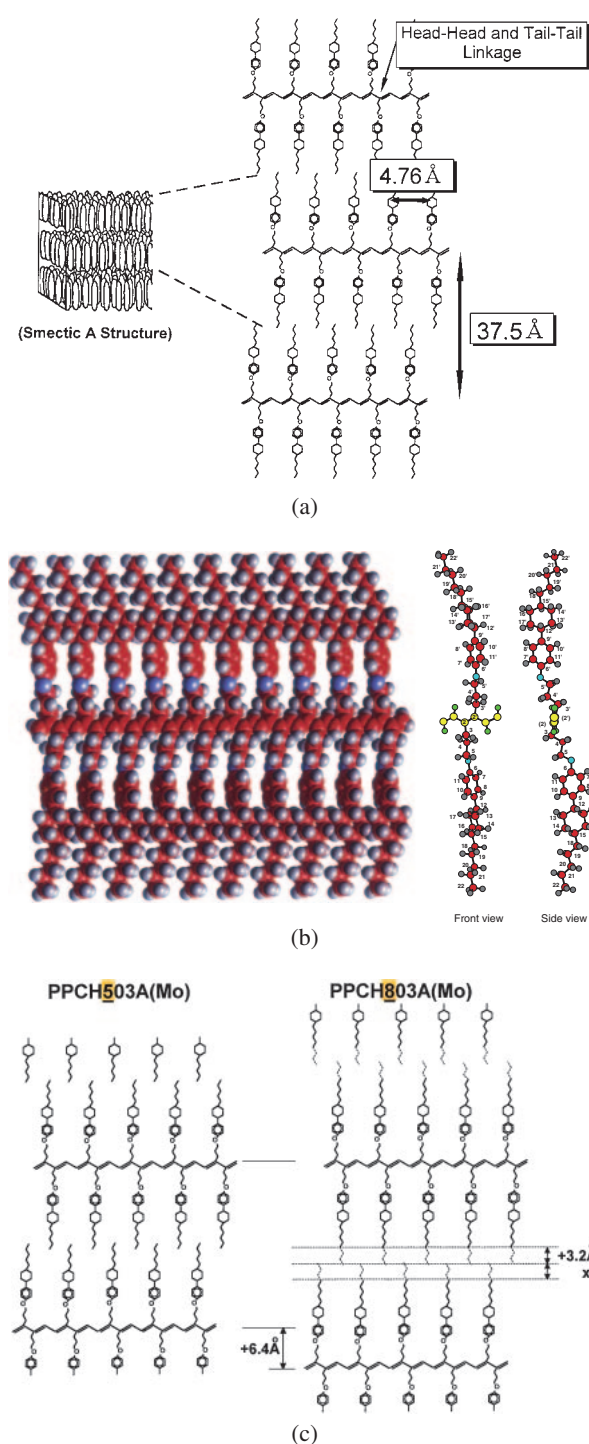


Fig. 6. (a) Higher order structure of Fe-based PPCH503A and smectic A structure. (b) Structure of PPCH503A optimized by molecular mechanics (MM) calculation on finite system (left site) (The red, gray, and purple balls indicate carbon, hydrogen, and oxygen atoms, respectively). The ball and stick figures drawn in the center and right sites are front and side views of the core parts of optimized structure, respectively (The carbon and hydrogen atoms in the main chain are expressed as yellow and green balls, in order to distinguish them from those of the side chain). (c) Comparison of inter-layer distance between PPCH503A and PPCH803A.

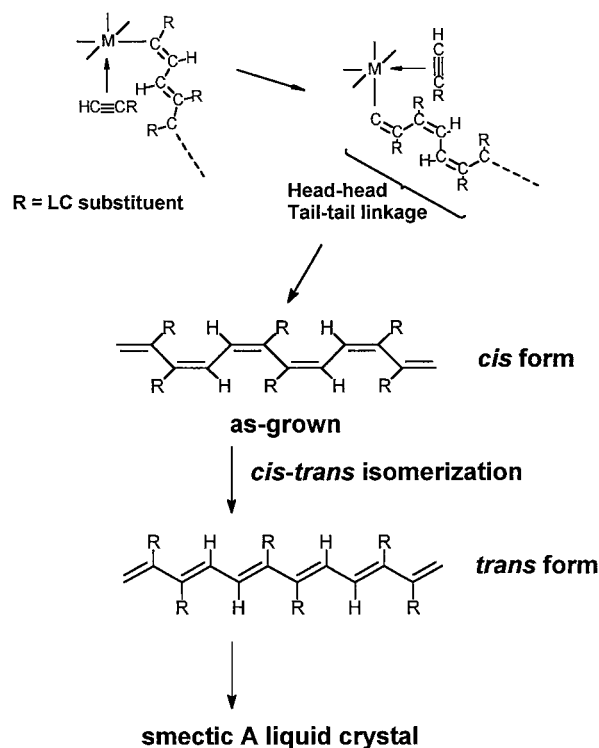


Fig. 7. Possible polymerization mechanism using Ziegler–Natta catalyst for LC-substituted acetylene and cis–trans isomerization.

Table 4. Absorption Band (λ_{\max}) and Intensity (ϵ_{\max}) and Proton Chemical Shift (δ) for PPCH n O3A and PBP503A

Catalyst	Polymer	λ_{\max} /nm ^a	ϵ_{\max} / $\times 10^3 \text{ M}^{-1} \text{ cm}^{-1}$ a)	δ /ppm ^b
Fe(acac) ₃ –	PPCH303A	324	2.0	5.98
AlEt ₃	PPCH503A	325	1.9	5.97
	PPCH803A	324	2.5	5.97
	PBP503A	insoluble		
MoCl ₅ –	PPCH303A	301	1.4	
Pn ₄ Sn	PPCH503A	301	1.4	no value
	PPCH803A	301	1.2	
	PBP503A	305	2.6	5.94–6.14

a) Absorption band due to $\pi \rightarrow \pi^*$ transition in conjugated polyene chain. b) Chemical shift of olefinic proton in cis form.

magnetic field was applied horizontal to photograph. The texture was aligned parallel to the magnetic field, although the alignment was not homogeneous. The incomplete alignment is attributed to an insufficient strength of the magnetic field (0.7–1.0 Tesla), which may cause a variation in σ and sample dependency, especially in the case of σ_{\perp} . In order to achieve complete alignment of the polymer in the highly viscous smectic LC state, a magnetic field strength of more than 2 Tesla is should be required.

3.6 Spin State and Chemical Doping. Figure 12 shows ESR spectra of the PCH and BP polymers in non-doped and iodine-doped states.^{16b} The results are also summarized in Table 6. In the non-doped state, the Fe-based PCH and BP polymers showed no signal, meanwhile the Mo-based PCH polymer showed two kinds of signals with g -values of 2.014

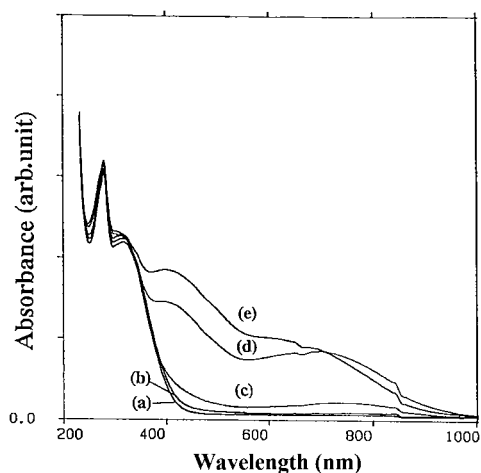


Fig. 8. Changes of UV-vis absorption spectra upon gas-phase iodine doping for the cast film of Fe-based PPCH503A. (a) intact; (b) 30 min; (c) 171 min; (d) 291 min; (e) 1131 min.

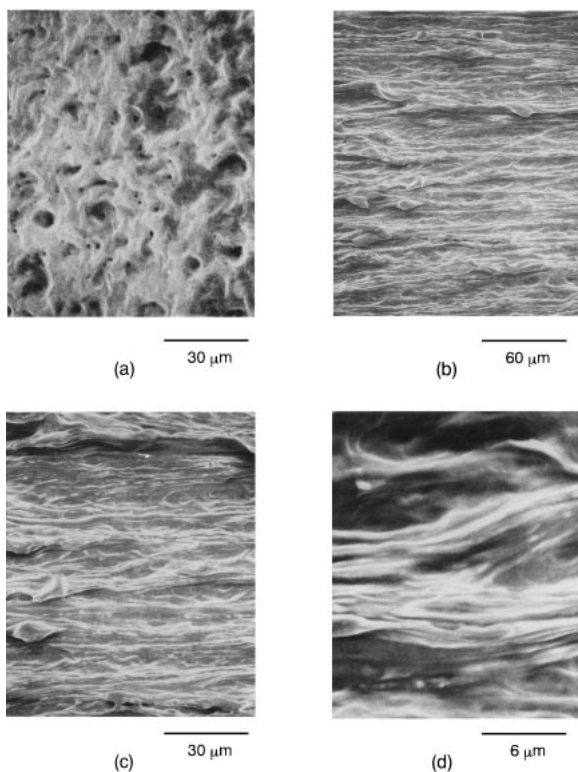


Fig. 9. SEM photographs of Fe-based PPCH503A. (a) no shear stress; (b)–(d) aligned with shear stress.

and 2.005. This is consistent with the above-mentioned result that the Fe-based Ziegler–Natta and the Mo-based metathesis catalysts produce cis and trans forms of mono-substituted polyacetylenes, respectively. Namely, the cis form is a kinetically favored product, and it easily isomerizes into a thermally more stable trans form during a thermal heating, chemical doping, or even polymerization using the metathesis catalyst. Such a cis–trans isomerization should cause defects in polyene chains, giving rise to unpaired electrons that are responsible for the paramagnetic behavior. In practice, upon the iodine doping,

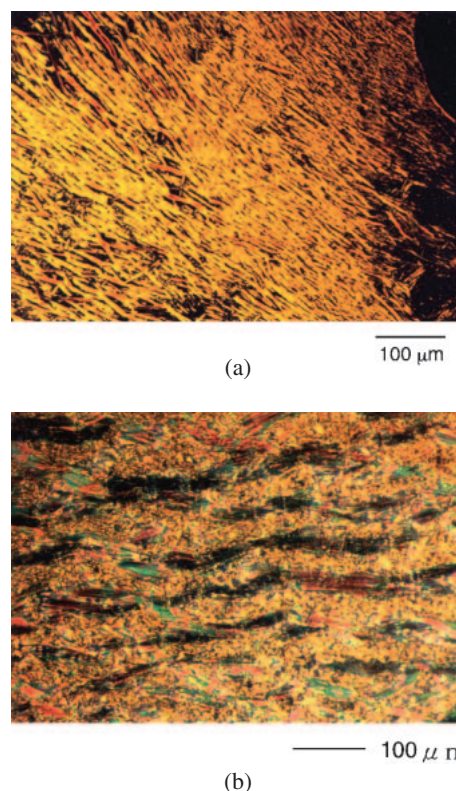


Fig. 10. Polarizing micrographs of (a) Mo-based PPCH503A aligned using shear stress, and (b) Fe-based PPCH803A aligned using a magnetic force field of 0.7 Tesla where magnetic field is parallel to the horizontal direction.

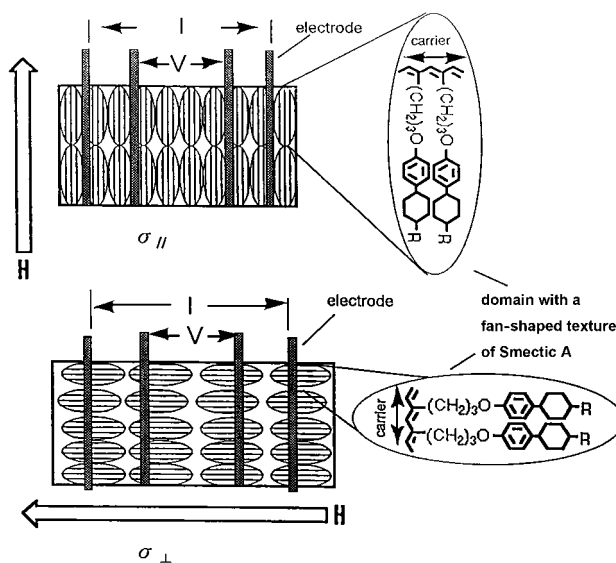


Fig. 11. Schematic representation of magnetically forced alignment of the side chain LC mono-substituted polyacetylene and sample cell for the four-probe method of electrical conductivity measurement (H is magnetic field).

the Fe-based PCH and BP polymers showed sharp ESR signals with g -values of 2.006 and 2.003, respectively. On the other hand, with the doped Mo-based polymer, the lower field signal ($g = 2.014$) slightly decreased in intensity and the higher field

Table 5. Electrical Conductivities ($\sigma/S\text{ cm}^{-1}$) for PPCH503A and PBP503A before and after Iodine Doping and Macroscopic Alignment

Catalyst ^{a)}	Polymer	Undoped	Iodine doped		
		σ	σ_{random}	σ_{\parallel}	σ_{\perp}
Fe	PPCH503A	10^{-11} – 10^{-10}	1.0×10^{-8}	1.3×10^{-6}	7.2×10^{-7}
Mo	PPCH503A	10^{-11} – 10^{-9}	1.3×10^{-7}	1.5×10^{-6}	1.4×10^{-11}
Fe	PBP503A	10^{-11} – 10^{-9}	1.0×10^{-8}	2.3×10^{-8}	1.2×10^{-10}

a) Fe: $\text{Fe}(\text{acac})_3\text{-AlEt}_3$, Mo: $\text{MoCl}_5\text{-Ph}_4\text{Sn}$.

Table 6. ESR Results of the Iodine-Doped LC Polyacetylene Derivatives

Catalyst	Polymer	<i>g</i> -Value	ΔH_{pp} ^{a)} /gauss	$\Delta H_{1/2}/\Delta H_{\text{pp}}$	Spin density /spins g^{-1}	<i>y</i> -Value ^{b)}
Fe	PPCH503A	2.006	15.1	2.05	3×10^{15}	0.065
Fe	PBP503A	2.003	11.0	2.36	1×10^{15}	0.097
Mo	PPCH503A	2.014, 2.005	— ^{c)}	— ^{c)}	2×10^{17}	0.028

a) ΔH_{pp} means a full width at maximum slope, corresponding to a peak to peak width in differential curve of signal. $\Delta H_{1/2}$ means a full width at half maximum. b) Dopant concentration defined as $[(\text{CHCR})^{+3y}(\text{I}_3^-)_x]_x$, where R is a liquid-crystal group. c) Two peaks are overlapped.

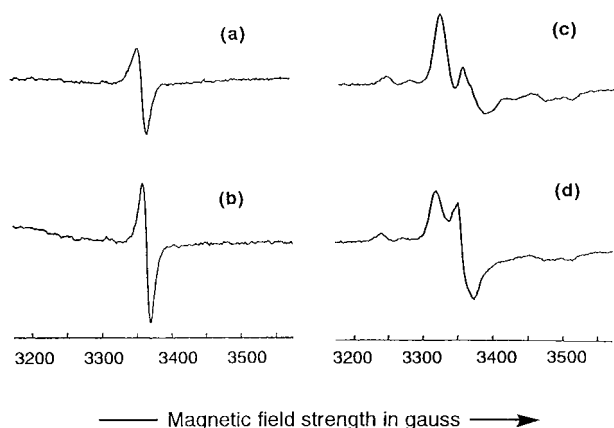


Fig. 12. ESR spectra measured at room temperature. (a) I_2 -doped PPCH503A (Fe); (b) I_2 -doped PBP503A (Fe); (c) non-doped PPCH503A (Mo); (d) I_2 -doped PPCH503A (Mo).

signal ($g = 2.005$) increased, resulting in overlapped signals as seen in Fig. 12.

The peak width, ΔH_{pp} , was 3–5 times larger, and the spin density was 2–4 orders of magnitude smaller than those of iodine-doped polyacetylene.²² Such a large peak width suggests that the unpaired electrons in the substituted polyacetylene tend to be more localized, probably due to a decrease in the planarity of the polyene chain. From the view point of electrical transport phenomenon, it can be argued that the present polymers have lower mobility and lower concentration of carriers. This may account for the lower electrical conductivity of the substituted polyacetylenes including the present PCH and BP polymers.

3.7 Orientation Behavior and Anisotropy under Magnetic Field. We measured fused state ^{13}C NMR spectra of side-chain LC polyacetylene derivatives as well as a LC acetylene monomer in isotropic and liquid-crystalline states to elucidate their orientation behaviors and anisotropies in chemical shifts.¹⁶

Measurements of the fused state ^{13}C NMR spectra were carried out on Bruker AMX-40 equipped with a high magnitude proton decoupler. The strength of magnetic field was 9.4 Tesla. The sample was first melted by heating and measured in the isotropic state. Then by applying the magnetic field, the sample was gradually cooled down with a temperature controller and measured in the LC state.

Figure 13 shows ^{13}C NMR spectra of PCH803A monomer in the isotropic and nematic phases. Upon the phase transition from the isotropic to LC phase, chemical shifts of aromatic carbons (C6–C9) of phenyl ring shifted to a lower magnetic field, down-field shift. Especially, those of C6 and C9 carbons showed relatively larger down-field shifts. The results are described in Fig. 14. On the other hand, chemical shifts of alkyne carbons of acetylene segments (C1 and C2) shifted to a higher magnetic field, up-field shift. The up-field shifts are also found in alkyl carbons of terminal group and methylene chain, although the degrees of the shifts are quite small. These tendencies in chemical shift become more remarkable as temperature decreases from 307 to 305 K, indicating an increase in degree of molecular orientation. Interestingly, the methylene carbon (C5) neighboring with the phenoxy moiety shows almost no change in chemical shift even after the phase transition. This suggests that the C5 carbon atom might be located in an axis which forms an angle of about 53.5° (magic angle) to the molecular axis.

Figure 15 shows ^{13}C NMR spectra of PPCH803A in the isotropic and smectic phases. The polymer in the smectic phase has a high viscosity and low fluidity, which causes a broadening of the signals. Upon the phase transition, the phenyl carbons (C6–C9) also show the down-field shifts. It is intriguing that the down-field shifts in the polymer are larger than in the case of the monomer, as summarized in Table 7. That is, the down-field shifts of C6, C9, and C7, C8 carbons of the polymer are 48–50 and 19–20 ppm, respectively. Whereas, those of the monomer are 37–40 and 15–17 ppm, respectively. The results imply that the LC state of the polymer gives a larger anisotropic environment than that of the monomer. This can

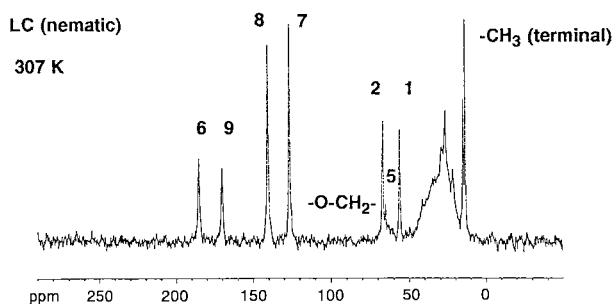
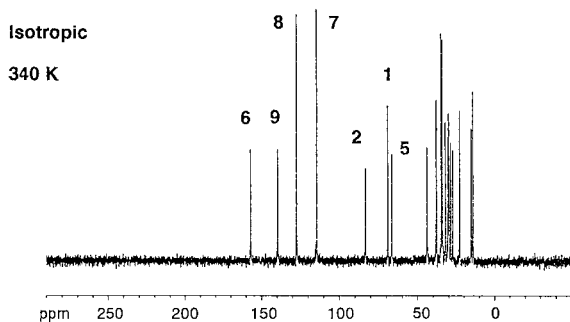
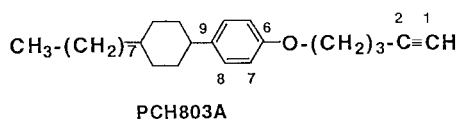


Fig. 13. ^{13}C NMR spectra of PCH803A in the isotropic (upper) and nematic (lower) states.

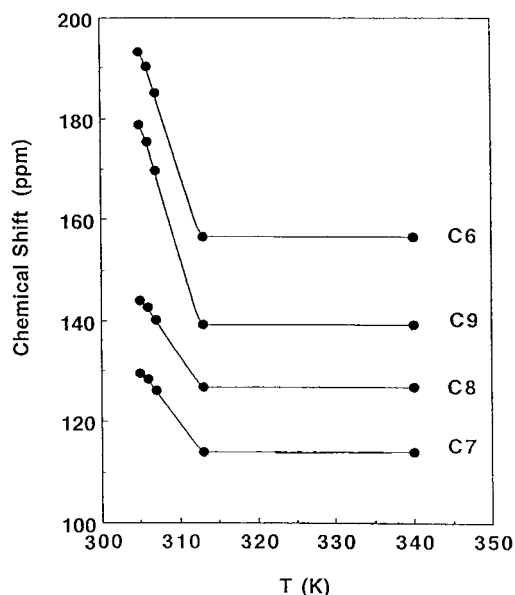
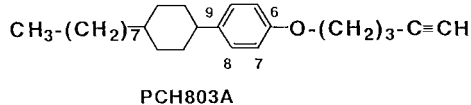


Fig. 14. ^{13}C NMR chemical shifts of phenylene ring of PCH803A in the isotropic and nematic states.

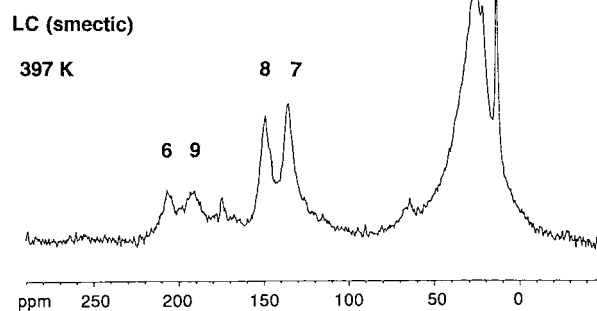
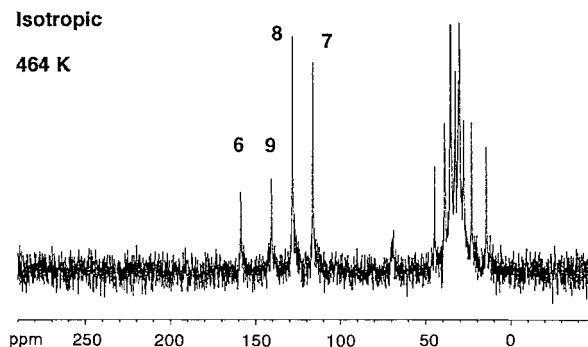
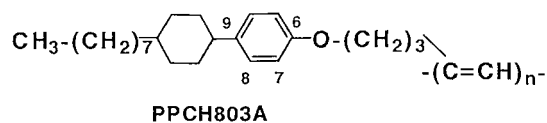
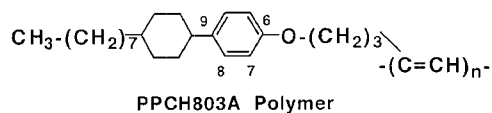


Fig. 15. ^{13}C NMR spectra of PPCH803A in the isotropic (upper) and smectic (lower) states.

Table 7. Changes of Chemical Shifts (ppm) upon Transition from the Isotropic to LC Phase for PCH803A and Fe-Based PPCH803A

	C6	C7	C8	C9	Terminal (Alkyl)
σ_{aniso}	206.6	135.0	148.4	190.5	12.4
σ_{iso}	158.3	115.8	127.7	140.2	14.1
$\Delta\sigma^{\text{a)}$	48.3	19.2	20.7	50.3	-1.7
$\Delta\sigma^{\text{a)}$ (Monomer)	36.6	15.5	17.0	39.5	-0.5

a) $\Delta\sigma = \sigma_{\text{aniso}} - \sigma_{\text{iso}}$.



be rationalized with a difference of LC phase between the polymer and the monomer where the former and the latter are respectively smectic and nematic phases. In other words, higher order and hence larger anisotropy are generated in the smectic phase, compared with the nematic phase.

We evaluated chemical shifts semi-quantitatively in the isotropic and anisotropic states by using the shielding tensors of a di-substituted benzene, 1-alkoxy-4-alkylbenzene, used as

a model compound. The calculated isotropic (σ_{iso}) and anisotropic (σ_{aniso}) chemical shifts were 157.4 and 191.3 ppm, respectively. The difference between them, defined as $\Delta\sigma = \sigma_{\text{aniso}} - \sigma_{\text{iso}}$, was 39.6 ppm. The down-field shift and its magnitude are consistent with the experimental results for PCH803A, where δ of the C6 carbon for instance was 36.6 ppm. Taking into account the electron density distributions of sp^3 , sp^2 , and sp hybrid carbon atoms in cartesian coordinates and chemical shift tensors reported so far, the largest shielding for aromatic carbons is perpendicular to the aromatic ring. For aliphatic carbons, however, the smallest shielding is perpendicular. The anisotropy in the shielding produces changes of chemical shifts observed upon the phase transition from the isotropic to LC states. The changes in the chemical shifts indicate that the monomer and the side chain of the polymers are oriented parallel to the direction of magnetic field employed in NMR measurement, which means that LC domains macroscopically aligned to give a mono domain structure as shown in Fig. 1.

We also evaluated orientational orders of LC states of the monomer and polymer. By correlating the order parameter with the change in chemical shift associated with the isotropic–anisotropic phase transition, we obtained the order parameter of the monomer, $S_{\text{mono}} = 0.38$ (307 K)–0.49 (305 K), and then derived a conventional formulae as follows:

$$S_{\text{poly}} = 1.26(S_{\text{mono}}). \quad (1)$$

Thus, the order parameter of the polymer, S_{poly} , was calculated to be 0.62 with $S_{\text{mono}} = 0.49$. The value of 1.26 in the above equation means that the orientational order increases upon the polymerization of LC monomer,¹⁸ and therefore, it can be regarded as an index of polymerization effect on the orientational order.

4. Conclusion

We synthesized two kinds of liquid-crystalline polyacetylene derivatives by using Fe-based Ziegler–Natta, Mo-based metathesis and Rh-based catalysts. The polymers had enantiotropic smectic A phases by virtue of a spontaneous orientation of LC side chain composed of phenylcyclohexyl or biphenyl mesogenic moieties. It was found from XRD measurements that the LC side chains alternate on both sides of the polyene chain, giving rise to a stereoregular sequence, such as head–head–tail–tail linkage. Electrical conductivities measured using a four-probe method were 10^{-8} – 10^{-7} S cm^{-1} upon iodine doping of the cast films of the polymers. The alignment of the main chain accompanied with the side chain orientation using an external magnetic force of 0.7–1.0 Tesla enhanced the electrical conductivity up to 10^{-6} S cm^{-1} and gave rise to a notable electrical anisotropy. It was shown from the fused state ^{13}C NMR measurements using a superconducting magnet of 9.4 Tesla that the LC side chains of the polymer were completely oriented along the magnetic field, giving a mono-domain structure.

The author is grateful to Professor Emeritus H. Shirakawa and Dr. H. Goto (University of Tsukuba) and Dr. K. Araya (Hitachi Ltd.) for their collaborations. Acknowledgements are also given to Prof. J. Isoya (University of Tsukuba) for

ESR measurements, Prof. A. Kawaguchi (Ritsumeikan University) for XRD analyses, and Dr. T. Nishizawa and Dr. K. Masuda (Kobe Steel Ltd.) for the fused state ^{13}C NMR measurements. This work was supported by a Grant-in-Aid for Science Research in a Priority Area, “Super-Hierarchical Structures” (No. 446) from the Ministry of Education, Culture, Sports, Science and Technology, Japan.

References

- a) T. Ito, H. Shirakawa, S. Ikeda, *J. Polym. Sci., Polym. Chem. Ed.* **1974**, *12*, 11. b) J. C. W. Chien, *Polyacetylene: Chemistry, Physics and Material Science*, Academic Press, Orlando, FL, **1984**, Chap. 2.
- a) H. Naarmann, N. Theophilou, *Synth. Met.* **1987**, *22*, 1. b) K. Akagi, M. Suezaki, H. Shirakawa, H. Kyotani, M. Shimomura, Y. Tanabe, *Synth. Met.* **1989**, *28*, D1. c) J. Tsukamoto, A. Takahashi, K. Kawasaki, *Jpn. J. Appl. Phys.* **1990**, *29*, 125.
- a) W. J. Trepka, R. J. Sonnenfeld, *J. Polym. Sci.* **1970**, *8*, 2721. b) R. J. Kern, *J. Polym. Sci.* **1969**, *7*, 621. c) C. I. Simionescu, V. Percec, *J. Polym. Sci., Polym. Symp.* **1980**, *67*, 43.
- a) S.-Y. Oh, R. Ezaki, K. Akagi, H. Shirakawa, *J. Polym. Sci., Part A: Polym. Chem.* **1993**, *31*, 2977. b) S.-Y. Oh, K. Akagi, H. Shirakawa, K. Araya, *Macromolecules* **1993**, *26*, 620. c) K. Akagi, S.-Y. Oh, H. Goto, Y. Kadokura, H. Shirakawa, *Trans. Mater. Res. Soc. Jpn.* **1994**, *15A*, 259. d) H. Shirakawa, Y. Kadokura, H. Goto, S.-Y. Oh, K. Akagi, K. Araya, *Mol. Cryst. Liq. Cryst.* **1994**, *255*, 213. e) K. Akagi, H. Goto, Y. Kadokura, H. Shirakawa, S.-Y. Oh, K. Araya, *Synth. Met.* **1995**, *69*, 13. f) H. Goto, K. Akagi, H. Shirakawa, S.-Y. Oh, K. Araya, *Synth. Met.* **1995**, *71*, 1899. g) K. Akagi, H. Goto, S. Fujita, H. Shirakawa, *J. Photopolym. Sci. Technol.* **1997**, *10*, 233. h) K. Akagi, H. Goto, J. Murakami, S. Silong, H. Shirakawa, *J. Photopolym. Sci. Technol.* **1999**, *12*, 269. i) H. Goto, S. Nimori, K. Akagi, *Synth. Met.* **2005**, *155*, 576.
- a) S.-H. Jin, S.-J. Choi, W. Ahn, H.-N. Cho, S.-K. Choi, *Macromolecules* **1993**, *26*, 1487. b) S.-J. Choi, S.-H. Jin, J.-W. Park, H.-N. Cho, S.-K. Choi, *Macromolecules* **1994**, *27*, 309. c) S.-J. Choi, S.-H. Kim, W. Ahn, H.-N. Cho, S.-K. Choi, *Macromolecules* **1994**, *27*, 4871.
- a) K. Akagi, H. Tanaka, R. Toyoshima, H. Shirakawa, *Trans. Mater. Res. Soc. Jpn.* **1994**, *15A*, 513. b) R. Toyoshima, M. Narita, K. Akagi, H. Shirakawa, *Synth. Met.* **1995**, *69*, 289. c) N. Koide, H. Iida, *Mol. Cryst. Liq. Cryst.* **1995**, *261*, 427. d) R. Toyoshima, K. Akagi, H. Shirakawa, *Synth. Met.* **1997**, *84*, 431. e) K. Akagi, M. Narita, R. Toyoshima, H. Shirakawa, *Mol. Cryst. Liq. Cryst.* **1998**, *318*, 157.
- a) F. Vicentini, J. Barrouillet, R. Laversanne, M. Mauzac, F. Bibonne, J. P. Parneix, *Liq. Cryst.* **1995**, *19*, 235. b) P. Ibison, P. J. S. Foot, W. Brown, *Synth. Met.* **1996**, *76*, 297.
- a) K. Akagi, J. Oguma, H. Shirakawa, *J. Photopolym. Sci. Technol.* **1998**, *11*, 249. b) K. Akagi, J. Oguma, S. Shibata, R. Toyoshima, I. Osaka, H. Shirakawa, *Synth. Met.* **1999**, *102*, 1287. c) J. Oguma, R. Kawamoto, H. Goto, K. Itoh, K. Akagi, *Synth. Met.* **2001**, *119*, 537. d) J. Oguma, K. Akagi, H. Shirakawa, *Synth. Met.* **1999**, *101*, 86. e) J. Oguma, X.-M. Dai, K. Akagi, *Mol. Cryst. Liq. Cryst.* **2001**, *365*, 331.
- a) R. Toyoshima, K. Akagi, H. Shirakawa, *Synth. Met.* **1997**, *84*, 431. b) I. Osaka, S. Shibata, R. Toyoshima, K. Akagi, H. Shirakawa, *Synth. Met.* **1999**, *102*, 1437. c) I. Osaka, H. Goto, K. Itoh, K. Akagi, *Synth. Met.* **2001**, *119*, 541. d) I. Osaka, H.

- Goto, K. Itoh, K. Akagi, *Mol. Cryst. Liq. Cryst.* **2001**, 365, 339.
- 10 a) H. Goto, K. Itoh, K. Akagi, *Synth. Met.* **2001**, 119, 351. b) H. Goto, K. Akagi, *Macromolecules* **2002**, 35, 2545.
- 11 a) K. Akagi, H. Goto, M. Okuda, H. Shirakawa, *Mol. Cryst. Liq. Cryst.* **1998**, 316, 201. b) H. Goto, K. Akagi, *Synth. Met.* **1999**, 102, 1292. c) R. Kiebooms, H. Goto, K. Akagi, *Synth. Met.* **2001**, 119, 117. d) H. Goto, K. Akagi, *Mol. Cryst. Liq. Cryst.* **2001**, 365, 491. e) H. Goto, K. Akagi, *J. Polym. Sci., Part A: Polym. Chem.* **2005**, 43, 616. f) R. Kiebooms, H. Goto, K. Akagi, *Macromolecules* **2001**, 34, 7989.
- 12 a) K. Akagi, H. Goto, H. Shirakawa, *Synth. Met.* **1997**, 84, 313. b) X.-M. Dai, H. Goto, K. Akagi, H. Shirakawa, *Synth. Met.* **1999**, 102, 1289. c) X.-M. Dai, H. Goto, K. Akagi, H. Shirakawa, *Synth. Met.* **1999**, 102, 1291. d) X.-M. Dai, H. Narihiro, H. Goto, K. Akagi, H. Yokoyama, *Synth. Met.* **2001**, 119, 397. e) X.-M. Dai, H. Goto, K. Akagi, *Mol. Cryst. Liq. Cryst.* **2001**, 365, 347. f) H. Narihiro, X.-M. Dai, H. Goto, K. Akagi, *Mol. Cryst. Liq. Cryst.* **2001**, 365, 363. g) X.-M. Dai, H. Narihiro, H. Goto, K. Akagi, H. Yokoyama, *Mol. Cryst. Liq. Cryst.* **2001**, 365, 355. h) H. Goto, X. Dai, H. Narihiro, K. Akagi, *Macromolecules* **2004**, 37, 2353. i) H. Goto, X. Dai, T. Ueoka, K. Akagi, *Macromolecules* **2004**, 37, 4783.
- 13 a) S.-Y. Oh, F. Oguri, K. Akagi, H. Shirakawa, *J. Polym. Sci., Part A: Polym. Chem.* **1993**, 31, 781. b) K. Akagi, H. Goto, K. Iino, H. Shirakawa, J. Isoya, *Mol. Cryst. Liq. Cryst.* **1995**, 267, 277. c) K. Iino, H. Goto, K. Akagi, H. Shirakawa, A. Kawaguchi, *Synth. Met.* **1997**, 84, 967.
- 14 a) K. Yoshino, K. Kobayashi, T. Kawai, M. Ozaki, K. Akagi, H. Shirakawa, *Synth. Met.* **1995**, 69, 49. b) K. Yoshino, K. Kobayashi, K. Myojin, T. Kawai, H. Moritake, M. Ozaki, K. Akagi, H. Goto, H. Shirakawa, *Mol. Cryst. Liq. Cryst.* **1995**, 261, 637. c) K. Yoshino, K. Kobayashi, K. Myojin, M. Ozaki, K. Akagi, H. Goto, H. Shirakawa, *Jpn. J. Appl. Phys.* **1996**, 35, 3964.
- 15 K. Akagi, H. Shirakawa, *Synth. Met.* **1993**, 60, 85.
- 16 a) K. Akagi, H. Goto, H. Shirakawa, T. Nishizawa, K. Masuda, *Synth. Met.* **1995**, 69, 33. b) K. Masuda, T. Nishizawa, K. Akagi, H. Shirakawa, *J. Mol. Struct.* **1998**, 441, 173.
- 17 a) H. Kuroda, H. Goto, K. Akagi, A. Kawaguchi, *Macromolecules* **2002**, 35, 1307. b) Y. Kurauchi, H. Miki, K. Akagi, A. Kawaguchi, *Polymer* **2004**, 45, 303.
- 18 a) K. Akagi, H. Shirakawa, *Macromol. Symp.* **1996**, 104, 137. b) K. Akagi, H. Shirakawa, *The Polymeric Materials Encyclopedia. Synthesis, Properties and Applications*, CRC Press, **1996**, Vol. 5, pp. 3669–3675. c) K. Akagi, H. Shirakawa, *Electrical and Optical Polymer Systems: Fundamentals, Methods, and Applications*, ed. by D. L. Wise, G. E. Wnax, D. J. Trantolo, T. M. Cooper, J. D. Gresser, Marcel Dekker, **1998**, Chap. 28, pp. 983–1010.
- 19 C. I. Simionescu, S. Dumitrescu, *J. Polym. Sci., Part A: Polym. Chem.* **1977**, 15, 2479.
- 20 P. S. Woon, M. F. Farona, *J. Polym. Sci., Polym. Chem. Ed.* **1974**, 12, 1749.
- 21 Y. Yang, M. Tabata, S. Kobayashi, K. Yokota, A. Shimizu, *Polym. J.* **1991**, 23, 1135.
- 22 D. Davidov, S. Roth, W. Neuman, H. Sixl, *Solid State Commun.* **1984**, 52, 375.



Professor Kazuo Akagi graduated from the Department of Hydrocarbon Chemistry of Faculty of Engineering at Kyoto University and earned a Doctoral degree in 1980. He became a Research Associate at Fukui University in 1982. He became an Assistant Professor in the Institute of Materials Science at University of Tsukuba in 1984, and then was promoted to Associate Professor in 1991 and Professor in 1998. He became a Director of Tsukuba Research Center of Interdisciplinary Materials Science in 2003 and a Professor of the Graduate School of Pure and Applied Sciences in 2004. He has been a Professor of the Graduate School of Engineering, Kyoto University since 2006. He is studying Materials Science, Polymer Chemistry, and Liquid Crystal Chemistry. Prof. Akagi was awarded The Divisional Award of The Chemical Society of Japan (1999), NISSAN Science Prize (2000), The Award of the Japanese Liquid Crystal Society for Outstanding Paper (2000), Tsukuba Prize (2001), The Award of the Society of Polymer Science, Japan (2002), The Commendation for Science and Technology by the Minister of Education, Culture, Sports, Science and Technology, Prizes for Science and Technology (2005). He is a Head Investigator of Scientific Research in Priority Area entitled “Control of Super-Hierarchical Structures and Innovative Functions of Next-Generation Conjugated Polymers,” Grants-in-Aids for Scientific Research in Japan.